A Direct and Fast Methodology for Ship Recognition in Sentinel-2 Multispectral Imagery

Heiselberg, Henning

Published in:
Remote Sensing

Link to article, DOI:
10.3390/rs8121033

Publication date:
2016

Document Version
Publisher's PDF, also known as Version of record

remote sensing

MDPI

Article

A Direct and Fast Methodology for Ship Recognition in Sentinel-2 Multispectral Imagery

Henning Heiselberg [1,2,*]

[1] National Space Institute, Technical University of Denmark, 2800 Kongens Lyngby, Denmark
[2] Joint Research & Test Centre, Danish Defense Acquisition & Logistics Org., Lautrupbjerg 1-5, 2750 Ballerup, Denmark

Academic Editors: Clement Atzberger and Prasad S. Thenkabail
Received: 22 September 2016; Accepted: 14 December 2016; Published: 19 December 2016

Abstract: The European Space Agency satellite Sentinel-2 provides multispectral images with pixel sizes down to 10 m. This high resolution allows for ship detection and recognition by determining a number of important ship parameters. We are able to show how a ship position, its heading, length and breadth can be determined down to a subpixel resolution. If the ship is moving, its velocity can also be determined from its Kelvin waves. The 13 spectrally different visual and infrared images taken using multispectral imagery (MSI) are "fingerprints" that allow for the recognition and identification of ships. Furthermore, the multispectral image profiles along the ship allow for discrimination between the ship, its turbulent wakes, and the Kelvin waves, such that the ship's length and breadth can be determined more accurately even when sailing. The ship's parameters are determined by using satellite imagery taken from several ships, which are then compared to known values from the automatic identification system. The agreement is on the order of the pixel resolution or better.

Keywords: Sentinel-2; multispectral; ship; recognition; identification; turbulent wake; Kelvin waves

1. Introduction

Marine situation awareness is of vital importance for monitoring, the control of piracy, smuggling, fisheries, irregular migration, trespassing, spying, traffic safety, shipwrecks, and also for the environment (oil or chemical dumping), etc. In cases of cooperative transponder systems, e.g., the automatic identification system (AIS), vehicle monitoring system (VMS) or long-range identification and tracking system (LRIT), they may not be transmitting deliberately or accidentally, they are able to be jammed, spoofed, and sometimes experience erroneous returns or are simply turned off. AIS satellite coverage at high latitudes is sparse which means that other means of non-cooperative surveillance systems are required such as, for example, satellite or airborne systems.

The Sentinel satellites under the Copernicus program provide excellent and freely available multispectral [1] and Synthetic Aperture Radar (SAR) imagery with resolutions down to 10 m. The orbital period is 10 days for the Sentinel-2 (S2) satellite A, with the image strips overlapping at an given point on the Earth, and the typical revisit period is five days in Europe, being more frequent in the Arctic. When the S2-B is launched, the revisit time for most of Europe will be two or three days. Unless it is obscured by clouds, the multispectral and SAR satellite imagery will provide frequent coverage of the Earth that increases with latitude, and this condition is particularly useful for arctic surveillance [2,3], ship detection [4–9], oil spills [10], crops and trees [11], as well as hyperspectral imaging [12].

This article focuses on S2 MSI ship detection, ship recognition, and ship identification. Detection is relatively easy due to the high sensitivity and the generally dark sea background. Recognition is based on high-resolution images, which allow for an accurate and robust determination of a ship's

position, and its length, breadth and form, heading and velocity. Finally, identification is possible from the 13 MSI spectral bands. The accuracy and confidence of all of this is reliant on the ship's spectral reflectances and the ship's size. The analysis and discussion of the accuracy of the recognition and identification from a ship's S2 MSI data return are the results of the S2 MSI detection, recognition and identification process.

The paper is organized such that the S2 data is described, followed by how it is then analyzed within the ship model. The complication of wakes and how they can be included in the modeling is also discussed. The ship model and analysis method used is described in the Appendix A. Results for ship parameters are given for a number of ships. Ship lengths and breadths have been compared to reported values by using AIS ground truth numbers and, finally, a discussion, summary and outlook are also offered.

2. Satellite Data and Ship Modeling

2.1. Sentinel-2 Data and Analysis

S2 carries the wide-swath, high-resolution, multispectral imager (MSI) with 13 spectral bands with 10, 20 and 60 m resolution [3]. We will mainly analyze the four bands with the 10 m resolution, namely B2 (blue), B3 (green), B4 (red) and B8 (near-infrared). The S2 images as shown here are almost cloud-free Level 1C recorded on 23 August 2016 (shown in Figure 1) and 5 September 2016; both were taken over Skagen, Denmark. Ships from other satellite MSI images have also been analyzed which confirm and support the conclusions of this article but they have not been included for reasons of brevity.

Figure 1. Sentinel-2A image tile VNK from 23 August 2016 at 10:30 a.m. UTC showing Skagen—the northernmost tip of Denmark. The image is RGB contrast-enhanced. A number of container and tanker ships (see Table 1) are moored just east of Skagen in the tranquil sea of Kattegat, a number of which are waiting for bulk fuel. Close to the coast a few clouds can be seen, with their shadows being cast northward.

A number of methods do exist for tracking, searching and signature analysis in visual and infrared imagery. We have developed dedicated Matlab software that enables us to search for, detect, and track objects such as ships at sea or aircraft in the sky. We restrict the search to open sea without clouds where objects such as ships are to be found. A smaller box is selected around each object as shown in Figure 2, which then constitutes a single ship image segment. The background is determined and subtracted in each band. Each ship image is then subsequently analyzed as described in Appendix A.

2.2. Ship Model and Parameters

The analysis is based on a basic ship model as shown in Figure 2. The ship's signature is established with an approximation made by the rectangular form of length L and breadth B, and rotated by heading angle θ. In a more precise analysis we also make a determination of the bow and Kelvin waves, and remove the turbulent wake effect.

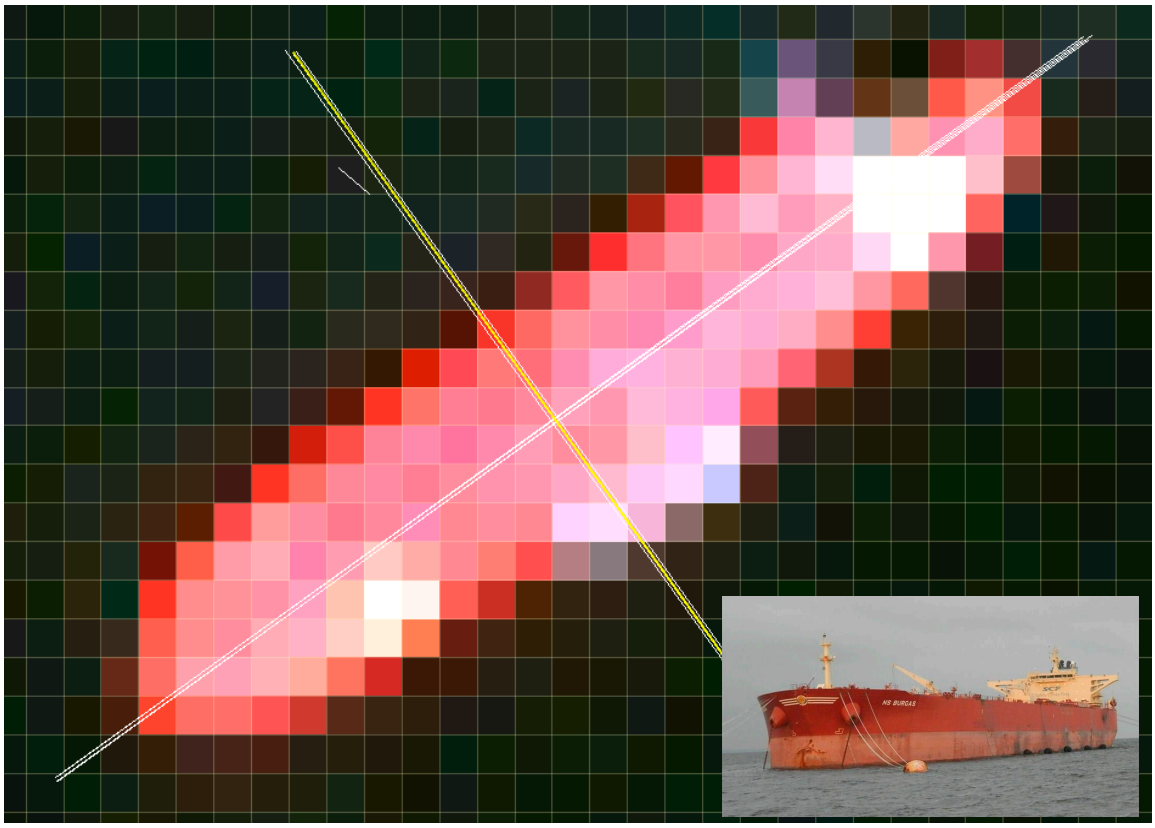

Figure 2. The RGB ship image box of NS Burgas (see Table 1, also present in Figure 1). Multiplying the pixels (i,j) by l = 10 m gives the ship coordinates (x,y). The axes show the ship axis coordinate system (x′,y′). Insert shows a horizontal visual image of the ship (with a substantially higher pixel resolution).

The ship images contains reflectances $I_c(i,j)$ for each of the multispectral bands (c). The pixel coordinates (i,j) are the (x,y) coordinates in units of the pixel resolution l, which is l = 10 m for the blue, green, red and near-infrared bands c = B2, B3, B4, and B8, respectively, but l = 20 m for the bands c = B5, B6, B7, B8a, B11, B12, and l = 60 m for c = B1, B9, B10. The total ship reflectivity in spectral band c is:

$$I_c = \sum_{i,j}^{>} I_c(i,j) \tag{1}$$

Once these as a background have been subtracted, the sum can run over all of the pixels on the ship image. However, due to wakes and clutter we apply a minimum threshold between the

background and ship reflectances, and only pixels with reflectances above this threshold are included. This is indicated by the >index above the sum. For all ships, one threshold is chosen well above the sea reflectance but well below typical ship reflectances. The ship parameters are found to decrease only slowly with increasing threshold for a wide region of threshold values.

If we alternatively just sum up the number of pixels with reflectances above the threshold,

$$A_c = l^2 \sum_{i,j}^{>} 1 \tag{2}$$

we ideally get the ship area $A_c = B{\cdot}L$, but generally it will depend on the threshold, spectral band, image clutter and pixel resolution. The two methods used are based on the reflectance and pixel counting and both are very useful, but we shall use (1) with a proper choice of threshold.

As described in Appendix A, the corresponding sums in Equations (1) and (2) of the reflectances weighted with pixel numbers i and j give the ship center-of-mass coordinates $(\overline{x}, \overline{y})$, when normalized with the total reflectance. Likewise, weighting with the moments i^2, j^2, and $i{\cdot}j$ gives the ship's covariances, from which the ship length (L), breadth (B) and orientation (θ) can be determined (see the formulas in Appendix A). From even higher moments (e.g., i^3, j^3, $i{\cdot}j^2$, etc.) one can also estimate asymmetries such as the ship's bow and other details of the ship's form. However, such higher moments are increasingly sensitive to clutter and wakes, and are threshold-dependent. As described in Appendix A, the model is similar to a principal component analysis but calculates the ship parameters directly.

Instead we find it useful, once the ship's heading angle θ has been determined and the ship axis is known, to transform to the ship axis coordinate system as shown in Figures 2 and 3. As described in Appendix A, one is then able to calculate the ship's breadth along the ship's axis, $B(x')$. A narrower ship's bow can be estimated from $B(x')$; consequently, from this its breadth and length can be determined much more precisely.

2.3. Turbulent Wakes and Kelvin Waves

A ship moving relative to the sea creates a turbulent wake with the breadth increasing as a function of the distance (r) behind the ship. In Reference [13] it is parameterized at long distances as

$$W(r) \approx 1.9\, B^{\frac{4}{5}} r^{\frac{1}{5}} \tag{3}$$

On the other hand, in Reference [14] the power scaling $r^{1/7}$ fits the turbulent wake of two warships better. The turbulent wakes are often very long and this is very useful for detecting and tracking ships with visual and infrared satellite images [13]. However, the turbulent wakes appear to be dependent on the ship type, breadth, length and speed, and therefore are not a very good determinations to use for the accuracy of a ship's breadth.

The wakes also reflect solar light which is very difficult to separate from the ship's reflectance [15]. The inclusion of turbulent wakes can also dramatically increase the ship's length if included. The multispectral differences between the wake and ship, in particular in the S2 near-infrared band c = 8, can, however, can be exploited to distinguish between the ship and its wake, as shown below.

A sailing ship also creates Kelvin waves bounded by cusp-lines separated by an angle of $\pm\arcsin(1/3) = \pm 19.47^\circ$ on each side of the referenced ship, as in Figure 3. The Kelvin wave length is related to the ship speed V as [16]

$$\lambda = \frac{2\pi V^2}{g} \tag{4}$$

where $g = 9.98\ \mathrm{m/s^2}$ is the gravitational acceleration at the surface of the Earth.

The cusps of the Kelvin waves lead to a larger apparent ship length and breadth. The amplitude of the Kelvin waves increases sternwards and will, as shown in Figure 5b below, appear as oscillations

in the breadth along the ship axis $B(x')$. Hereby the Kelvin waves can effectively be removed and the wavelength determined.

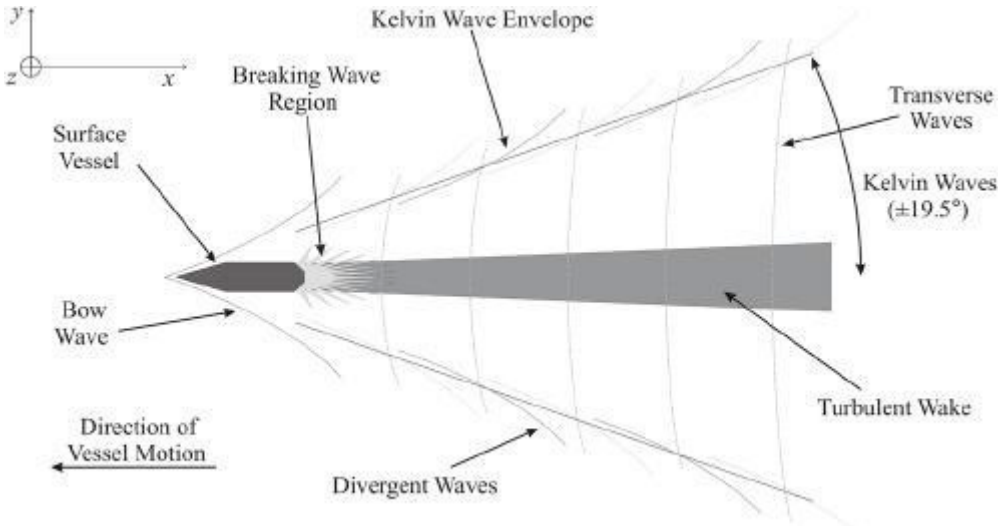

Figure 3. Sketch of Kelvin waves and turbulent wake from a sailing ship.

3. Results

The S2 multispectral images are analyzed by using dedicated and bespoke developed Matlab software for this purpose. The processing time is mainly for searching for ships, which can take seconds depending on the complexity and size of the mega- to giga-pixel 12 bit images. For each of the detected ships, as shown in Figure 1, a box is then drawn around the ship, and the reflectances, center of mass system coordinates and covariances are calculated in the described ship model as described in Appendix A. The calculation of the ship parameters is extremely simple and fast.

3.1. Multispectral Signatures

A typical medium-sized ship L = 100 m and B = 20 m appears in ca. 20 pixels for each of the high-resolution bands c = B2, B3, B4, B8, as well as in fewer pixels for the other bands. The collected multispectral ship signature data as shown in Figure 1 contains just over 100 data points, which can be exploited as ship "fingerprints" for identification. As expected, the sea is dark and mainly reflects in the blue band c = 2. Ships, wakes and clouds have high radiances for all spectral bands c = 2, 3, 4; however, ships often reflect a color different from white as, e.g., seen in Figure 2. More interestingly, ships and land tend to reflect or emit more infrared light than wakes. Therefore, the high-resolution near-infrared band c = B8 is particularly useful for discriminating between the ship and wake, which then allows for a more accurate determination of the ship's length.

Clouds are seen in Figure 1 to cast shadows displaced ca. 570 m northward due to the solar elevation. In Skagen, at a 57°43′ latitude on 23 August, two months or 360°·2/12 = 60° after summer solstice, the solar elevation above the horizon is 57.7–23.44cos(60°) = 46°. The cloud altitude is therefore 570 m/tan(46°) = 550 m. The cloud shadows are also slightly displaced westward as seen from the sun-synchronous S2. Ship reflectances can also be affected by shadows, especially in the winter months at higher latitudes. In fact, a darker reflectance can be seen in Figure 2 at the ship's starboard stern (northward), which is most likely to be a shadow cast by the ship bridge.

3.2. Ship's Total Reflectance, Position, Heading, Length, and Breadth

The ship parameters for large- and medium-sized ships in the two Skagen datasets including Figure 1 are shown in Table 1. The total ship reflectance is panchromatic, i.e., summed over RGB

bands c = B2 + B3 + B4 and ship pixels. The calibration factor for standard radiation units W/sr may be calculated. Due to currents along the coast, most moored ships head southwest and south in the two datasets. Ship ellipticities are in most cases $\varepsilon \geq 0.90$, and high ellipticity is a good ship classifier.

Table 1. Ship parameters for the ships in S2 Figure 1: reflectance (I), heading angle (θ), ellipticity (ε), length (L) and breadth (B), see Appendix A. Numbers in parentheses are lengths and breadths found from reported values in the AIS ship data.

Ship	I_{2+3+4}	θ	ε	L (m)	B (m)
NS Burgas	26,370	33°	0.913	240 (275)	51 (48)
Eagle Barents	32,976	21°	0.912	252 (276)	55 (46)
GijonKnutsen	9939	17°	0.950	187 (183)	30 (27)
MarmaraMariner	2827	4°	0.968	130 (129)	17 (17)
Trade Navigator	2738	11°	0.963	125 (118)	17 (16)
Afines Sky	8013	19°	0.949	152 (162)	24 (23)
Skaw Provider	818	28°	0.966	110 (95)	15 (15)
Loireborg	2997	33°	0.955	113 (122)	17 (14)
Solstraum	2880	23°	0.899	89 (94)	21 (18)
Fjellstraum	2134	1°	0.950	94 (100)	15 (16)
BW Yangtze	14,530	33°	0.951	204 (229)	32 (32)
StenFjell	4343	−84°	0.921	131 (149)	27 (24)
SCL Basilia	4130	−97°	0.947	127 (140)	21 (22)
Karen Knutsen	20,809	−91°	0.914	256 (274)	54 (50)
Edith Kirk	6208	−100°	0.939	171 (183)	30 (27)
Grumant	5256	−104°	0.966	147 (181)	19 (23)
ChampionTrader	4223	−85°	0.975	185 (189)	21 (30)
Wilson Mersin	1412	−74°	0.942	84 (107)	15 (15)
Voorneborg	4590	−69°	0.944	116 (132)	20 (16)
Coral Monactis	1765	−69°	0.885	74 (95)	18 (15)
AtlanticaHav	358	−50°	0.845	53 (82)	15 (11)
Coral Obelia	741	−49°	0.930	83 (93)	16 (15)
Coral Pearl	3201	−60°	0.934	105 (115)	19 (19)
HHL Amur	8078	25°	0.920	128 (138)	26 (21)
HDW Herkules	1615	−88°	0.819	53 (54)	17 (10)
Elly Kynde	165	0°	1	17 (19)	≈5 (5)
Gottskar	434	0°	1	17 (21)	≈5 (6)
Frank Maiken	1081	18°	0.485	26 (18)	16 (6)
Haukur [1]	5366	−7°	0.878	95 (75)	24 (13)
Ritz Dueodde [1]	525	28°	0.904	32 (15)	7 (5)
Torland [1]	14,076	−1°	0.930	183 (140)	35 (22)
Sea Endurance [2]	4350	11°	0.731	90 (110)	35 (18)
Bow Triumph [2]	11,227	2°	0.852	162 (183)	46 (32)

[1] Sailing ship and includes ship wake. [2] Includes adjacent fueling ships.

The ship lengths and breadths as referenced in Table 1 are plotted in Figure 4, which are generally in good agreement between those found in the ship model using S2 data and the ground truth numbers from AIS. A few special cases disagree for obvious reasons. Three ships are sailing and the generated wake extends the ship length. Two ships have fueling ships docked alongside them which extends their breadth. By excluding these ships we are then able to calculate the standard deviation for the lengths $\sigma(L_{sat} - L_{GT}) = 16$ m and breadths $\sigma(B_{sat} - B_{GT}) = 3.8$ m between the S2 satellite data and the AIS ground truth. The S2 ship lengths are, on average, shorter than the ground truth lengths, which we attribute to the ship's bow and stern. Both extend the ship's length. We are able to find a best fit when the ship's length is extended with half of the ship's breadth. The resulting standard deviation is reduced to $\sigma(L_{sat} + B/2 - L_{GT}) = 10$ m. Geometrically the extension depends on the bow and stern angles with respect to the ship's axis. Bow lengths around half the breadth are compatible with most ship constructions. The corrected values and resulting 10 m standard deviation in ship length are representative as they are the same for the two datasets separately.

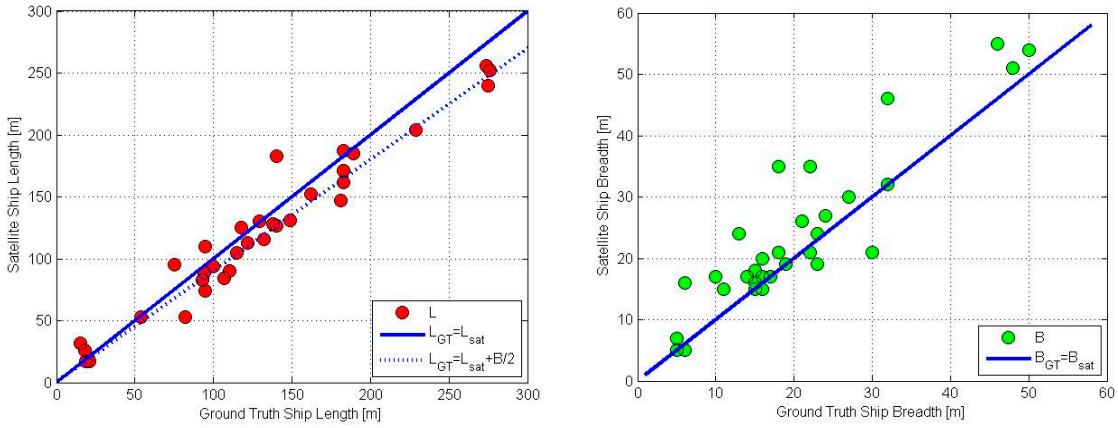

(**a**) (**b**)

Figure 4. (**a**) Ship lengths and (**b**) breadths. The ground truth lengths and breadths are from AIS ship records. The satellite lengths and breadths are the calculated values as used in the model given in Table 1. Blue lines indicate agreement whereas dashed line includes bow corrections as described in text.

Ships longer than ca. 30 m are seen in six pixels which is a minimum requirement in order to determine the six ship parameters: total reflectance, position, heading, length and breadth (I_c, $(\overline{x}, \overline{y})$, θ, B, L). The limited pixel resolution adds its own uncertainty, and the results become more dependent on the threshold. For example, in Table 1 the two small sail boats are detected in two pixels only, the ship's breadth is simply an assumed half a pixel. Small ships can only be detected in S2 images. For large- and medium-sized ships longer than ca. 30 m, we find that the ship model is robust and accurate for determining ship parameters.

3.3. Wake Removal and Ship Speed

In Figure 5a, a S2 panchromatic image of a sailing ship is shown. In Figure 5b, the corresponding ship breadth $B(x')$ (see Appendix A) is shown along the ship axis coordinate x'. One observes the ship breadth and wake width to be around 6·l = 60 m, with an increasing oscillation added on due to Kelvin wave cusps. A Fourier transform yields the wave number, which in turn gives the Kelvin wave length $\lambda \approx 5.5 \cdot l = 55\ m$. According to Equation (4), the ship speed is $V = 9.3\ m/s = 18\ kts$.

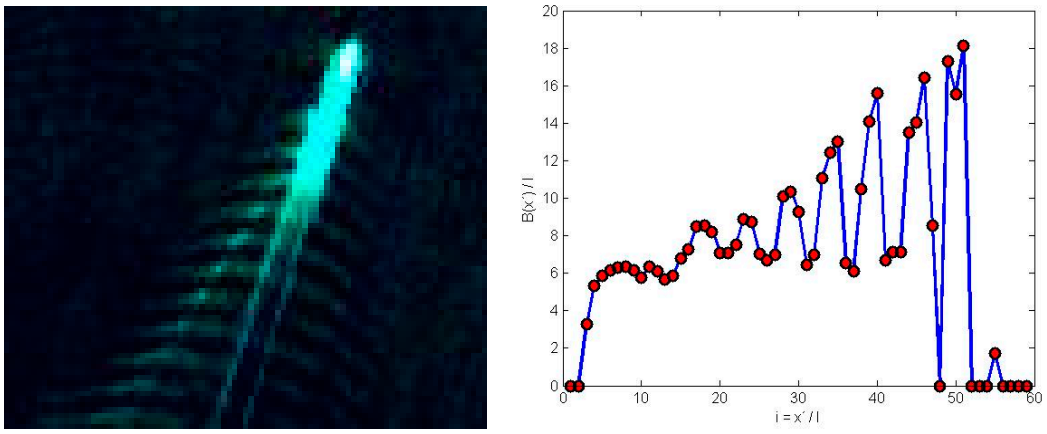

(**a**) (**b**)

Figure 5. (**a**) Ship with Kelvin waves and turbulent wake; (**b**) Corresponding ship breadth B(x') along ship axis x' including wake oscillations.

The ship length cannot be accurately determined from the panchromatic plot in Figure 5a, because the turbulent wake and Kelvin waves contribute to the ship breadth B(x) at a substantial length behind the ship. We find that the wake is reduced in the high-resolution near-infrared B8 and we also find that shorter ship lengths are better in agreement with ground truth lengths.

The ship's bow can also be estimated from $B(x)$. It increases from 0 to 6·l in around three pixels, and therefore the bow length is ≈3·l = 30 m, which is also half of the ship's breadth. Therefore, half of this bow length should be added to the ship's length L in order to obtain the ground truth length.

Ship maneuvers do not affect the ship's breadth $B(x')$ because the ship heading is automatically corrected for in the ship's axis coordinate system. Strong side winds may cause asymmetries in wakes and waves but do not change the Kelvin wavelengths.

4. Discussion

Ship detection, recognition and identification in S2 MSI has been analyzed. The images allow for the detection of even small ships. Recognition and determination of ship parameters require that the ship extend over several pixels, which for S2 data requires medium-sized ships above ca. 30 m. The ship parameters of position, length, breadth, and heading can all be reliably determined as can the ship's speed when Kelvin waves are found. Length estimations can be improved by determining the bow length as well as correcting for shadows. The ship lengths deviate from reported AIS numbers with a standard deviation of 16 m without bow corrections, but 10 m for ship lengths with bow corrections. The standard deviation is 3.8 m for ship breadths. These deviations are on the order of or less than the S2 pixel resolution. The high resolution and the 13 multispectral bands' information are able to identify most medium- and large-sized ships.

The detection of sailing ships is simpler, due to the long turbulent wakes and Kelvin waves behind the ship; however, their reflectances do complicate the determination of ship parameters. By exploiting the multispectral information in the reflectances, in particular the smaller near-infrared reflectance of wakes as compared to most ships, one can separate ships from wakes and determine the ship lengths more accurately. For medium- and large-sized ships it is useful to determine the ship axis and plot the breadth along this axis. Thereby one can separate the Kelvin waves and determine the ship breadth, bow length, Kelvin wavelength and speed more accurately.

In Reference [16], the ship lengths for 53 vessels were determined from Geo-Eye-1 satellite images with a higher resolution l = 2 m. Their segmentation method differs from the ship model employed here specifically on wake removal. Their optimized method results in a standard deviation between the satellite and ground truth ship lengths of 26 m. This may seem large considering the high resolution but most of the ships are seafaring and wake removal seems difficult.

5. Conclusions and Outlook

S2 MSI is very useful for the detection, recognition of ship parameters larger than ca. 30 m, and detailed identification of ships. If the ship reflectances in the 13 multispectral bands have been recorded for all ship pixels and stored in a database, this will enable the reflectances to serve as "fingerprints" for later identification. When Sentinel-2B is launched, the revisit time will be a few days in Europe and almost daily in the Arctic. S2 MSI will greatly improve the marine situational awareness, especially for non-cooperative ships—weather permitting. For example, in September 2016 Crystal Serenity was the first cruise ship that risked sailing along the Northwest Passage which is infested with unchartered reefs and titanic icebergs. The ship is non-cooperative since satellite AIS coverage is very limited at these latitudes.

An obvious extension of these first results for ship classification from MSI is the discrimination of ice floes in the Arctic and to develop methods for automatic ship searches in an Arctic environment. In future work we will apply all 13 multispectral bands using pansharpening or hypersharpening techniques [17] for the bands with lower resolution in order to improve the classification, discrimination and multispectral identification of ships and threats from icebergs.

Additionally, a comparison to Sentinel-1 SAR imagery will provide complementary and weather-independent information but with a lower resolution (except in the rare and narrow swath SM GRD full resolution mode). Also SAR is unable to detect low dielectric glass fiber boats. The synergy of S1 and S2 imagery should be investigated for daily searching and tracking.

Acknowledgments: We are grateful for many useful comments from the referees.

Conflicts of Interest: The author declare no conflict of interest.

Appendix A. Determination of Ship Parameters

The total ship reflectance I_c in band c is given by the sum in Equation (1). Inserting factors of i and j in this sum, and normalizing it with the total reflectance, we obtain the ship cms coordinates:

$$\overline{x} = \frac{l}{I_c} \sum_{i,j}^{>} i \cdot I_c(i,j) \tag{A1}$$

$$\overline{y} = \frac{l}{I_c} \sum_{i,j}^{>} j \cdot I_c(i,j) \tag{A2}$$

Likewise, inserting factors i^2, j^2 and $i \cdot j$, the ship covariances are:

$$\sigma_{xx}^2 = \frac{l^2}{I_c} \sum_{i,j}^{>} i^2 \cdot I_c(i,j) \; - \overline{x}^2 \tag{A3}$$

$$\sigma_{yy}^2 = \frac{l^2}{I_c} \sum_{i,j}^{>} j^2 \cdot I_c(i,j) \; - \overline{y}^2 \tag{A4}$$

$$\sigma_{xy}^2 = \frac{l^2}{I_c} \sum_{i,j}^{>} i \cdot j \cdot I_c(i,j) \; - \; \overline{x} \cdot \overline{y} \tag{A5}$$

It is convenient to translate the coordinates into the ship cms coordinates (x',y') rotated by the ship heading angle θ such that the ship is aligned along the x'-axis (see Figure 2):

$$x - \overline{x} = \; x' \, cos(\theta) - y' sin(\theta) \tag{A6}$$

$$y - \overline{y} = x' \, sin(\theta) + y' cos(\theta) \tag{A7}$$

At the first approximation, we assume that the ship bow is short. The ship is then a simple rectangle of length L and breadth B, and the ship extends from: $-L/2 < x' < L/2$ and $-B/2 < y' < B/2$. The corresponding ship covariances in the (x',y') coordinate systems are: $\sigma_{x'x'}^2 = \; L^2/12, \sigma_{y'y'}^2 = \; B^2/12$ and $\sigma_{x'y'}^2 = 0$, when the ship is large compared to the pixel resolution. The covariances σ_{xx}^2, σ_{yy}^2 and σ_{xy}^2 are now found by replacing the pixel coordinates $i = x/l$ and $j = y/l$ in Equations (A3)–(A5) as given in Equations (A1) and (A2). We obtain

$$\sigma_{xx}^2 = \frac{1}{12} \left(L^2 \cos(\theta)^2 + \; B^2 \sin(\theta)^2 \right) \tag{A8}$$

$$\sigma_{yy}^2 = \frac{1}{12} \left(B^2 \cos(\theta)^2 + \; L^2 \sin(\theta)^2 \right) \tag{A9}$$

$$\sigma_{xy}^2 = \frac{1}{12} \left(L^2 - \; B^2 \right) sin(\theta) \, cos(\theta) \tag{A10}$$

It is now straightforward to determine the three ship parameters L, B and θ from the three covariances σ_{xx}, σ_{yy} and σ_{xy}. Firstly, the ship heading angle is given by

$$tan(2\theta) = \frac{2\sigma_{xy}^2}{\sigma_{xx}^2 - \sigma_{yy}^2} \tag{A11}$$

Next we introduce the ship ellipticity $\epsilon = \left(L^2 - B^2 \right) / \left(L^2 + B^2 \right)$. It can be expressed and calculated in terms of the covariances as

$$\epsilon = \frac{L^2 - B^2}{L^2 + B^2} = \frac{\sigma_{xx}^2 - \sigma_{yy}^2}{\sigma_{xx}^2 + \sigma_{yy}^2} \frac{1}{\cos(2\theta)} \tag{A12}$$

The ship ellipticity is usually between $\epsilon \approx 0.89$–0.96, corresponding to the length/breadth ratio $L/B = \sqrt{(1+\epsilon)/(1-\epsilon)} \approx 4-7$, and can be used for classifying elongated ship-like objects. It discriminates ships from icebergs, ice floes, wind turbines and other less-elongated objects.

The ship breadth and length squared can now be conveniently expressed as:

$$\mathrm{B}^2 = 6(1-\epsilon)(\sigma_{xx}^2 + \sigma_{yy}^2) \tag{A13}$$

$$\mathrm{L}^2 = 6(1+\epsilon)(\sigma_{xx}^2 + \sigma_{yy}^2) \tag{A14}$$

The model described here is similar to principal component analysis in 2D (2DPCA). The symmetry axes are aligned with the principal eigenvectors, and L and B are related to the principal eigenvalues. The model described is simpler, faster and able to calculate the ship parameters directly. The 2DPCA analysis is more elaborate and complicated and it can provide more eigenvalues which, in our case, has not been necessary, given we only have ground truth values for ship lengths and breadths from AIS.

In most of the S2 images, the background is dark sea, and consequently a threshold is able to be set between sea and ship reflectances. Moving ships, however, create turbulent wakes and Kelvin waves, which do have an effect on the calculated reflectance. These can effectively be removed by calculating the ship breadth $B(x')$ along the ship axis x'. For simplicity, let us assume that we have aligned the x and x' axes (i.e., $\theta = 0$). In that case, the variance in the y' (or y) direction is

$$\sigma(i)^2 = \frac{l^2}{I_c} \sum_{j}^{>} j^2 \cdot I_c(i,j) \; - \overline{y}^2 \tag{A15}$$

as function of the pixel i = x/l along the ship axis. The corresponding ship breadth is (cf. Figure 5b)

$$B(x') = \sqrt{12} \cdot \sigma(i) \tag{A16}$$

References

1. ESA Sentinel-2 Delivers First Images. Available online: http://www.esa.int/Our_Activities/Observing_the_Earth/Copernicus/Sentinel-2/Sentinel-2_delivers_first_images (accessed on 7 January 2016).
2. Krogager, E.; Heiselberg, H.; Møller, J.G.; von Platen, S. Fusion of SAR and EO imagery for Arctic surveillance. In Proceedings of the NATO IST-SET-128 Specialist Meeting, Norfolk, VA, USA, 4–5 May 2015.
3. Brekke, C.; Weydahl, D.J.; Helleren, Ø.; Olsen, R. Ship traffic monitoring using multipolarisation satellite SAR images combined with AIS reports. In Proceedings of the 7th European Conference on Synthetic Aperture Radar (EUSAR), Friedrichshafen, Germany, 2–5 June 2008.
4. Daniel, B.; Schaum, A.; Allman, E.; Leathers, R.; Downes, T. Automatic ship detection from commercial multispectral satellite imagery. *Proc. SPIE 8743* **2013**. [CrossRef]

5. Burgess, D.W. Automatic ship detection in satellite multispectral imagery. *Photogramm. Eng. Remote Sens.* **1993**, *59*, 229–237.
6. Zhu, C.; Zhou, H.; Wang, R.; Guo, J. A novel hierarchical method of ship detection from spaceborne optical image based on shape and texture features. *IEEE Trans. Geosci. Remote Sens.* **2010**, *48*, 3446–3456. [CrossRef]
7. Corbane, C.; Marre, F.; Petit, M. Using SPOT-5 HRG data in panchromatic mode for operational detection of small ships in tropical area. *Sensors* **2008**, *8*, 2959–2973. [CrossRef] [PubMed]
8. Corbane, C.; Najman, L.; Pecoul, E.; Demagistri, L.; Petit, M. A complete processing chain for ship detection using optical satellite imagery. *Int. J. Remote Sens.* **2010**, *31*, 5837–5854. [CrossRef]
9. Tang, J.; Deng, C.; Huang, G.-B.; Zhao, B. Compressed-domain ship detection on spaceborne optical image using deep neural network and extreme learning machine. *IEEE Trans. Geosci. Remote Sens.* **2015**, *53*, 1174–1185. [CrossRef]
10. Gade, M.; Hühnerfuss, H.; Korenowski, G. *Marine Surface Films*; Springer: Heidelberg, Germany, 2006.
11. Immitzer, M.; Vuolo, F.; Atzberger, C. First experience with Sentinel-2 data for crop and tree species classifcations in Central Europe. *Remote Sens.* **2016**, *8*, 166. [CrossRef]
12. Eismann, M.T. Hyperspectral Remote Sensing. *SPIE* **2012**, *PM210*, 748.
13. Lapierre, F.D.; Borghgraef, A.; Vandewal, M. Statistical real-time model for performance prediction of ship detection from microsatellite electro-optical imagers. *EURASIP J. Adv. Signal Process.* **2009**, *2010*, 1–15. [CrossRef]
14. Golbraikh, E.; Eidelman, A.; Soloviev, A. On the helical behavior of turbulence in the ship wake. *J. Hydrodyn. Ser. B* **2013**, *25*, 83–90. [CrossRef]
15. Bouma, H.; Dekker, R.J.; Schoemaker, R.M.; Mohamoud, A.A. Segmentation and Wake Removal of Seafaring Vessels in Optical Satellite Images. *Proc. SPIE* **2013**, *8897*. [CrossRef]
16. Thomson, W. On ship waves. *Proc. Inst. Mech. Eng.* **1887**, *38*, 409–434. [CrossRef]
17. Selva, M.; Aiazzi, B.; Butera, F.; Chiarantini, L.; Baronti, S. Hyper-sharpening: A first approach on SIM-GA data. *IEEE J. Sel. Top. Appl. Earth Obs. Remote Sens.* **2015**, *8*, 3008–3024. [CrossRef]